Thermodynamic functions, freezing transition, and phase diagram of dense carbon-oxygen mixtures in white dwarfs

Hiroshi Iyetomi, Shuji Ogata, and Setsuo Ichimaru
Department of Physics, University of Tokyo, 7-3-1 Hongo, Bunkyo-ku, Tokyo 113, Japan
(Received 6 September 1988; revised manuscript received 17 March 1989)

Equations of state for dense carbon-oxygen (C-O) binary-ionic mixtures (BIM's) appropriate to the interiors of white dwarfs are investigated through Monte Carlo simulations, by solution of relevant integral equations and variational calculations in the density-functional formalism. It is thereby shown that the internal energies of the C-O BIM solids and fluids both obey precisely the linear mixing formulas. We then present an accurate calculation of the phase diagram associated with freezing transitions in such BIM materials, resulting in a novel prediction of an azeotropic diagram. Discontinuities of the mass density across the azeotropic phase boundaries are evaluated numerically for application to a study of white-dwarf evolution.

I. INTRODUCTION

Binary-ionic mixtures (BIM's) of carbon and oxygen are thought to constitute the internal composition of the white dwarfs produced by helium burning; such a white dwarf in a close binary system may make a likely progenitor of a Type-I supernova (SNI).[1-3] It has been noted[4-6] that a dense matter in the interior of a white dwarf may undergo a freezing transition as its density and/or inverse temperature increase through the evolutionary processes.

An outstanding problem associated with such a solidification is the phase diagram or a possibility of chemical separation in the BIM material. Stevenson[7] showed how sensitive the phase diagram of carbon-oxygen (C-O) mixtures was to the assumptions of thermodynamic models, and in particular pointed out a possibility of a *eutectic* phase diagram when the random-alloy mixing (RAM) model was assumed for the internal energies in the solid phase. This prediction of a eutectic was then followed by proposal of new models for white-dwarf cooling, luminosity, and SNI mechanisms involving chemical separation.[8,9]

As for a theoretical study of chemical separation, Barrat *et al.*[10] used a density-functional approach to analyze freezing of binary hard-sphere mixtures into disordered crystals and found in particular that the phase diagram can be of a *spindle* type, an *azeotropic* type, or a eutectic type, depending on the ratio between the hard-sphere radii. Smithline and Haymet[11] developed a density-functional theory for the freezing of 1:1 hard-sphere mixtures and predicted three different stable solid phases: a disordered (phase separated) fcc structure and ordered CsCl and NaCl structures, depending on the hard-sphere radius ratio.

Recently, two of the present authors[12] presented a nonlinear density-functional approach to the crystallization of a classical one-component plasma (OCP), through microscopic analyses of the role played by the three-body or angular correlations. A simplified density-wave theory of freezing was thereby obtained.

In this paper, we extend the aforementioned OCP freezing theory to microscopic calculations of the phase diagram for the C-O BIM appropriate to the white-dwarf interior. To complement those analytic calculations, we further carry out a Monte Carlo (MC) simulation study of the BIM fluids and solids, and thereby elucidate salient features in their equations of state.

Contents of the paper are organized as follows: In Sec. II, after surveying the ranges of the physical parameters involved, we show through the MC analyses that the internal energies of the C-O BIM solids and liquids both accurately obey the linear mixing (LM) formulas, rather than the RAM formulas, invalidating thus the basic assumption introduced in Stevenson's eutectic diagram.[7] We then carry out the hypernetted chain (HNC) and the improved HNC (IHNC) calculations[13] on the C-O BIM fluids and prove again superiority of the LM formula. In Sec. III, we perform nonlinear density-functional calculations of the BIM solids, to derive an analytic expression for the mixing entropy; for liquids, we take the ideal entropy of mixing.[14] Those evaluations of internal energies and entropies lead to a novel prediction[15] of an azeotropic phase diagram for the C-O BIM materials in Sec. IV. Mindful of an application to the evolution calculations, we evaluate numerically the mass-density differences on the phase boundaries in Sec. V. Concluding remarks are given in Sec. VI.

II. THERMODYNAMIC FUNCTIONS FOR BIM MATERIALS

We consider a C-O BIM with $x = n_O/n$ (the molar fraction of oxygen), where $n = n_C + n_O$ is the number density of ions. The mass densities are assumed in the range, $10^6 \le \rho_m \le 10^{10}$ g/cm^3, so that for the electronic pressure, $10^{10} \le P_e \le 10^{16}$ Mbar. The dimensionless density parameter of the electrons,[16]

$$r_s = 1.75\rho_m^{-1/3} , \tag{1}$$

ranges in $10^{-3} \le r_s \le 10^{-2}$; hence, the electrons form a relativistically degenerate, incompressible background of

negative charges, except across the phase boundaries, where $\Delta\rho_m/\rho_m < 10^{-3}$ (cf. Sec. V). The freezing temperatures of carbon plasmas,[17]

$$T_C = 3.48\times 10^4 r_s^{-1}\mathrm{K}\ , \tag{2}$$

are found in $2\times 10^6 \le T_C \le 5\times 10^7$ K.

The effective Coulomb coupling constant of the BIM is formulated as[16]

$$\Gamma = \langle Z^{5/3}\rangle \Gamma_e\ , \tag{3}$$

where $\langle Z^p\rangle = Z_1^p(1-x)+Z_2^p x$, and

$$\Gamma_e = 5.0476\times 10^{-2}\Gamma_m T_C/T\ . \tag{4}$$

We take $Z_1=6$ and $Z_2=8$ for the C-O BIM and $\Gamma_m=180$ for a transition to a bcc crystal in the classical OCP.[17]

A. MC simulation study

We have performed a series of MC simulations with $N=1024$, the number of MC particles, for the fluid and crystalline BIM's at various combinations of T and x, following the standard Metropolis algorithm.[18] In the simulations, we have implemented a possibility of interchanging two neighboring MC particles, in addition to the usual random displacements of particle positions. In the bcc lattice simulations, irrespective of the initial configurations, we have found the equilibrated final states to take random bcc-solid configurations. In Fig. 1, the resulting partial radial-distribution functions, $g_{\mu\nu}(r)$ with $\mu,\ \nu=$C, O, are shown for the parameters relevant to white-dwarf interiors.

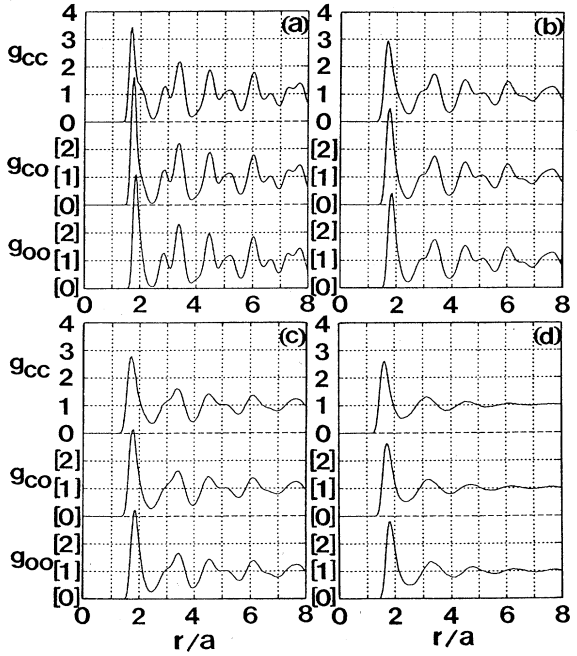

FIG. 1. Partial radial-distribution functions vs distance in units of $a=(3/4\pi n)^{1/3}$, the average interionic separation. (a) Lattice simulation at $T/T_C=0.5$ and $x=0.5$; (b) lattice simulation at $T/T_C=0.9$ and $x=0.5$; (c) lattice simulation at $T/T_C=1.1$ and $x=0.61$; (d) fluid simulation at $T/T_C=1.1$ and $x=0.48$.

With the knowledge of $g_{\mu\nu}(r)$ the (normalized) excess internal energy, $u=U_{ex}/Nk_BT$, is calculated as[16]

$$u=\sum_{\mu,\nu}\frac{\sqrt{n_\mu n_\nu}}{2k_BT}\int d\mathbf{r}\frac{Z_\mu Z_\nu e^2}{r}[g_{\mu\nu}(r)-1]\ . \tag{5}$$

The MC values of u are listed in Table 1 of Ref. 15 for fluid and random bcc-solid simulations.

In terms of the OCP excess internal-energy formula, $u_{OCP}(\Gamma)$, the ion-sphere model considerations[19,20] predict the LM formula:

$$u_{LM}=(1-x)u_{OCP}(Z_1^{5/3}\Gamma_e)+xu_{OCP}(Z_2^{5/3}\Gamma_e)\ . \tag{6}$$

The RAM model assumes that the internal energy of a BIM may be given by that of an equivalent OCP with $Z=\langle Z\rangle$, so that

$$u_{RAM}=u_{OCP}(\langle Z\rangle^{5/3}\Gamma_e)\ . \tag{7}$$

The OCP excess internal-energy formulas are

$$u_{OCP}(\Gamma)=-0.895\,929\Gamma+1.5+3225/\Gamma^2 \tag{8}$$

for the bcc crystalline state[21] and

$$u_{OCP}(\Gamma)=-0.898\,004\Gamma+0.967\,86\Gamma^{1/4}+0.220\,703\Gamma^{-1/4}-0.860\,97 \tag{9}$$

for the fluid state.[17]

In Table 1 of Ref. 15, we have compared the excess internal-energy values predicted by the mixing formulas (6) and (7) with the MC values. We have thus observed that the LM formula (6) can reproduce the MC values very accurately both in the fluid and solid states, while the RAM formula (7) is not accurate enough to be used in the phase-diagram calculations.

B. HCN and IHNC analyses

The excess internal energy of a BIM fluid can be calculated analytically through a solution to a set of integral equations such as the HNC and IHNC schemes.[13,16] Exact relations between the pair-correlation functions, $h_{\mu\nu}(r)=g_{\mu\nu}(r)-1$, and the direct correlation functions, $c_{\mu\nu}(r)$, are

$$g_{\mu\nu}(r)=\exp[-v_{\mu\nu}(r)+h_{\mu\nu}(r)-c_{\mu\nu}(r)+B_{\mu\nu}(r)]\ , \tag{10}$$

$$h_{\mu\nu}(r)=c_{\mu\nu}(r)+\sum_\lambda n_\lambda\int d\mathbf{r}' h_{\mu\lambda}(|\mathbf{r}-\mathbf{r}'|)c_{\lambda\nu}(r')\ , \tag{11}$$

where $v_{\mu\nu}(r)=Z_\mu Z_\nu e^2/k_BTr$, and $B_{\mu\nu}(r)$ are the bridge functions. In the HNC approximation, one assumes $B_{\mu\nu}(r)=0$ in Eq. (10).

In the IHNC scheme,[13] we evaluate the bridge functions approximately as

$$B_{\mu\nu}(r)=f_{\mu\nu}(r)B_{\mu\nu}^{(2)}(r)\ , \tag{12}$$

where

$$B^{(2)}_{\mu\nu}(r)=\tfrac{1}{2}\sum_{\lambda,\xi} n_\lambda n_\xi \int d\mathbf{r}_1 d\mathbf{r}_2 h_{\mu\lambda}(|\mathbf{r}-\mathbf{r}_1|) \times h_{\lambda\xi}(|\mathbf{r}_1-\mathbf{r}_2|) h_{\xi\mu}(|\mathbf{r}_2-\mathbf{r}|) \times h_{\lambda\nu}(r_1) h_{\xi\nu}(r_2) , \quad (13)$$

$$f_{\mu\nu}(r)=\left[\frac{B_{\mu\nu}(0)}{B^{(2)}_{\mu\nu}(0)}-1\right]\exp\left[-\left[\frac{r}{\sigma_{\mu\nu}}\right]^2\right]+1 . \quad (14)$$

The parameters are defined and calculated as

$$\sigma_{\mu\nu}=(\sigma_\mu+\sigma_\nu)/2 , \quad (15)$$

$$\sigma_\mu=1.8[3Z_\mu/4\pi(Z_1 n_1+Z_2 n_2)]^{1/3} , \quad (16)$$

$$B_{\mu\nu}(0)=H_{\mu\nu}(0)+c_{\mu\nu}(0)+1 , \quad (17)$$

and the screening potentials[16,20] at the origin are given by

$$H_{\mu\nu}(0)=0.9\Gamma_e[(Z_\mu+Z_\nu)^{5/3}-Z_\mu^{5/3}-Z_\nu^{5/3}] \quad (18)$$

in the ion-sphere model.

To examine accuracy of the HNC and IHNC schemes in predicting the thermodynamic properties of BIM systems, we have solved those sets of integral equations for $Z_1=1$ and $Z_2=2$ at $x=\frac{1}{2}$; the results are compared in Fig. 2 with the MC data obtained by Hansen *et al.*[22] We here find that the IHNC scheme in particular reproduces the MC data accurately.

We next examine accuracy and validity of the LM formula (6) for C-O BIM fluids in the HNC and IHNC schemes. In Fig. 3, we plot the values of $\Delta u \equiv u-u_{\rm LM}$ calculated in both schemes at $\Gamma_e=9$ as functions of x, and compare them with the ideal entropy of mixing in the BIM fluid,[14]

$$\Delta S_F(x)=\Delta S_{\rm id}(x)-Nk_B[(1-x)\ln(Z_1/\langle Z\rangle) + x\ln(Z_2/\langle Z\rangle)] , \quad (19)$$

with

$$\Delta S_{\rm id}(x)=-Nk_B[(1-x)\ln(1-x)+x\ln x] . \quad (20)$$

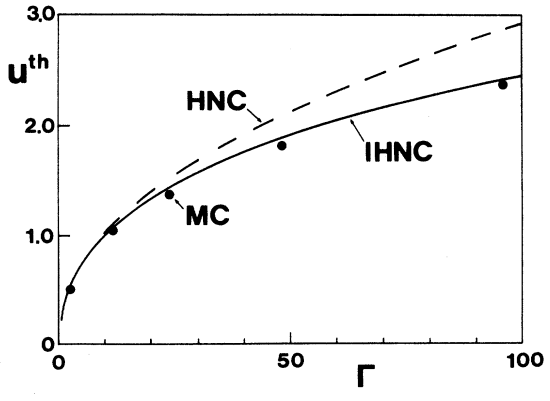

FIG. 2. Comparison of the thermal part, $u^{\rm th}=u+0.9\Gamma$, of the excess internal energy between the HNC and IHNC predictions and MC data (Ref. 22) for $Z_1=1$ and $Z_2=2$ with $x=0.5$.

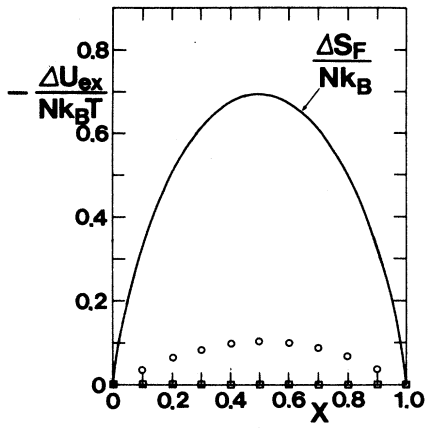

FIG. 3. The values of $\Delta u=u-u_{\rm LM}$ in the HNC (open squares) and IHNC (open circles) calculations for C-O fluids at $\Gamma_e=9$. The solid curve depicts Eq. (19) for comparison.

The second term of (19) stems from the charge neutrality condition in the uniform background of the electrons; at $x=0.5$, it amounts to a 1.5% correction to the first term. The deviations Δu are less than 10^{-3} for the HNC and 10^{-1} for the IHNC, smaller by far than the magnitude of $\Delta S_F/Nk_B$. These results have shown again the superiority of the LM formula (6) with the HNC and IHNC schemes.

III. ENTROPY OF MIXING FOR BIM SOLIDS

The normalized Helmholtz free energy, $f\equiv F/Nk_BT$, is expressed as $f=1.5+u-S/Nk_B$, where S is the entropy. In this section we are concerned with an evaluation of this entropy for a BIM solid; in BIM fluids, the entropy of mixing is given by Eq. (19).

A. Density-functional formalism

The free energy of a BIM solid is formulated as a functional of inhomogeneous density distributions $\rho_\mu(\mathbf{r})$ of carbon ($\mu=$C) and oxygen ($\mu=$O) atoms:

$$F[\rho_\mu(\mathbf{r})]=F_{\rm O}[\rho_\mu(\mathbf{r})]-\Phi[\rho_\mu(\mathbf{r})] , \quad (21)$$

where

$$F_{\rm O}[\rho_\mu(\mathbf{r})]=k_BT\sum_\mu \int d\mathbf{r}\,\rho_\mu(\mathbf{r})\{\ln[\Lambda_\mu^3\rho_\mu(\mathbf{r})]-1\} , \quad (22)$$

$$\Lambda_\mu=(2\pi\hbar^2/m_\mu k_BT)^{1/2} . \quad (23)$$

The interaction part of the free-energy functional, $\Phi[\rho_\mu(\mathbf{r})]$, is expanded with respect to density variation,

$$\delta\rho_\mu(\mathbf{r})=\rho_\mu(\mathbf{r})-\rho_\mu , \quad (24)$$

around the average (fluid) density ρ_μ, so that

$$\Phi[\rho_\mu(\mathbf{r})]=\Phi[\{\rho_\mu\}]+k_BT\sum_\mu\int d\mathbf{r}\,c_\mu^{(1)}(\mathbf{r};\{\rho_\mu\})\delta\rho_\mu(\mathbf{r})+\frac{k_BT}{2!}\sum_{\mu,\nu}\int d\mathbf{r}_1 d\mathbf{r}_2 c_{\mu\nu}^{(2)}(\mathbf{r}_1,\mathbf{r}_2;\{\rho_\mu\})\delta\rho_\mu(\mathbf{r}_1)\delta\rho_\nu(\mathbf{r}_2)+\cdots . \quad (25)$$

Here, $\{\rho_\mu\}=(\rho_C,\rho_O)$, and

$$c_{\mu_1}^{(n)\cdots\mu_n}(\mathbf{r}_1,\ldots,\mathbf{r}_n;\{\rho_\mu\})$$

is the n-body direct-correlation function[12] evaluated in the homogeneous (fluid) state.

B. Variational parameters

We now introduce basic assumptions in the treatment of the free-energy density-functional (25): A Gaussian parametrization of the local one-particle density variation is adopted so that

$$\rho_\mu(\mathbf{r};\gamma_\mu)=\left[\frac{\gamma_\mu}{\pi}\right]^{3/2}\sum_{j\in\{L_\mu\}}\exp(-\gamma_\mu|\mathbf{r}-\mathbf{r}_j|^2) , \quad (26)$$

where the j summation is carried out over the lattice sites $\{L_\mu\}$ for the μ particles. Assuming $\gamma_\mu a^2\gg 3.3$ where $a=(3/4\pi n)^{1/3}$, we take the Lindeman parameters[12] γ's as variational parameters.

Following the simplified density-wave theory obtained in Ref. 12 for the OCP, we truncate Eq. (25) at the terms involving $c_{\mu\nu}^{(2)}(\mathbf{r}_1,\mathbf{r}_2;\{\rho_\mu\})$; those terms are then evaluated through reduction by 78% of the second-shortest bcc reciprocal-lattice vector (RLV) contributions. The second direct-correlation functions for the fluid state are calculated in the IHNC scheme.

For characterization of a BIM solid, we introduce a third variational parameter ζ, describing the degree of a long-range order in the alloy.[23] We do so by decomposing the bcc crystal into two equivalent simple-cubic (sc) sublattices, "M" and "N", corresponding to the "Cs" and "Cl" sites in CsCl structures. The order parameter is thus defined as

$$\zeta\equiv\begin{cases}\dfrac{y_\mu-x_\mu}{x_\mu}=\dfrac{y_\nu-x_\nu}{1-x_\nu} & (x_\mu\le x_\nu) ,\\ \dfrac{y_\nu-x_\nu}{x_{ny}}=\dfrac{y_\mu-x_\mu}{1-x_\mu} & (x_\mu>x_\nu) ,\end{cases} \quad (27)$$

where x_μ denotes the molar fraction of μ atoms and y_μ refers to the fractional number of "M" sites occupied by the μ atoms. It is apparent that the order parameter ranges in $0\le\zeta\le 1$. That $\zeta=0$ means a randomly occupied alloy, while $\zeta=1$ corresponds to a state with a completely ordered alloy.

C. Variational calculations

Let $P(\mu,M)$ be the probability of finding a μ atom on a "M" site; this probability along with three other probabilities defined analogously is expressible in terms of ζ and x's. A Fourier component of the density distribution of the μ atoms is then calculated as

$$\tilde{\rho}_\mu(\mathbf{q})=(N/2)P(\mu,M)\delta_{\mathbf{q},\mathbf{G}}\exp(-q^2/\gamma_\mu)+(N/2)P(\mu,N)\delta_{\mathbf{q},\mathbf{G}}\exp(i\mathbf{q}\cdot\boldsymbol{\Delta}-q^2/\gamma_\mu) , \quad (28)$$

where $\mathbf{G}$ are the RLV's of the sc sublattices, $\boldsymbol{\Delta}=(d/2)(1,1,1)$, and d is the bcc lattice constant. An expression analogous to Eq. (28) applies for the ν atoms. We remark in passing that the random-alloy model of Barrat *et al.*[10] is recovered if $\zeta=0$ is set in those expressions.

We substitute inverse Fourier transforms of Eq. (28) in Eqs. (22) and (25). Equation (21) thus yields an expression for the free energy in the crystalline state, $F_C(x;\gamma_C,\gamma_O,\zeta)$, of the BIM solid in the Gaussian density-wave model. The increment of the free energy in mixing is given by

$$\Delta F(\gamma_C,\gamma_O,\zeta)=F_C(x;\gamma_C,\gamma_O,\zeta)-[(1-x)F_C(x=0)+xF_C(x=1)] . \quad (29)$$

That part of Eq. (29) arising from the ideal free energy (22) may be split into two separate contributions: $\Delta F_0=\Delta F_0(\infty)+\Delta F_0(\gamma)$, where

$$\Delta F_0(\infty)/Nk_BT=\tfrac{1}{2}\sum_{z,Z}P(z,Z)\ln P(z,Z) , \quad (30)$$

$$\Delta F_0(\gamma)/Nk_BT=\tfrac{3}{2}\left[(1-x)\ln\left[\frac{\gamma_C(x)}{\gamma_C(x=0)}\right]+x\ln\left[\frac{\gamma_O(x)}{\gamma_O(x=1)}\right]\right] . \quad (31)$$

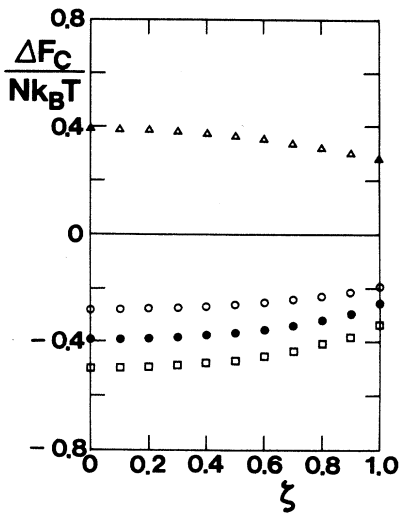

FIG. 4. Elements of variational minima, ΔF_C (solid circles) $=\Delta F_0(\infty)$ (open squares) $+\Delta F_0(\gamma)$ (open circles) $-\Delta\Phi$ (open triangles) of Eq. (29) at $\Gamma_e=9$ as functions of ζ for C-O BIM solids with $x=0.2$.

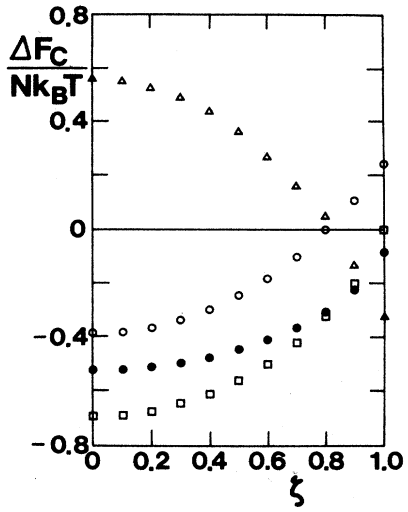

FIG. 5. Same as Fig. 4, but with $x=0.5$.

The part, $\Delta F_0(\infty)$, in which the summation is carried out over the particle species "z" and the sites "Z", represents the configurational entropy of mixing; $\Delta F_0(\gamma)$ describes changes of the γ's due to mixing.

The mixing entropy ΔS_C of the crystalline state is defined and calculated from the variational minimum ΔF_C of Eq. (29) with respect to γ_C, γ_O, and ζ as

$$\Delta S_C = -\Delta F_C/T \ . \tag{32}$$

Salient features in the results of these variational analyses for the BIM solids are summarized in the following.

Figures 4–6 plot the values of the elements in $\Delta F_C=\Delta F_0(\infty)+\Delta F_0(\gamma)-\Delta\Phi$ at $\Gamma_e=9$ as functions of ζ for the C-O BIM solids with $x=0.2$, 0.5, and 0.8. As these figures illustrate, the γ-dependent contributions in ΔF_0 acts to stabilize the random-alloy phase ($\zeta=0$). In

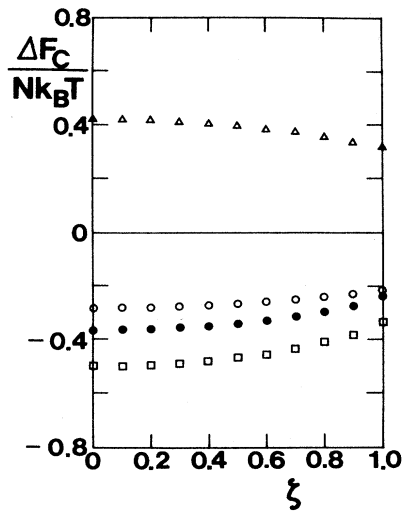

FIG. 6. Same as Fig. 4, but with $x=0.8$.

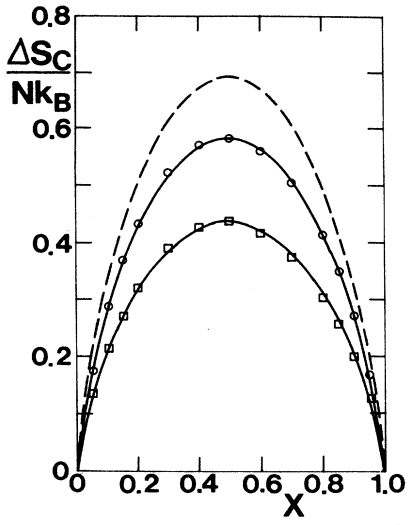

FIG. 7. The mixing entropies computed at minima of Eq. (29) vs x: open circles, $\Gamma_e=7$; open squares, $\Gamma_e=13$. The solid curves depict Eq. (33) at the same Γ_e values; the dashed curve, Eq. (20).

the parameter domain investigated, that is, $7\le\Gamma_e\le13$, such a random-alloy phase turns out to be stable for all the composition x.

The values of γ_C and γ_O at the variational-minimum conditions are as follows (in units of the average interionic separation a):

$$14\le\gamma_C\le19, \quad 20\le\gamma_O\le34 \quad \text{at } \Gamma_e=7 \ ,$$

$$32\le\gamma_C \text{ and } \gamma_O\le50 \quad \text{at } \Gamma_e=13 \ .$$

Finally we plot in Fig. 7 the values of ΔS_C computed variationally at $\Gamma_e=7$ and 13. We thus find that the calculated values can be parametrized accurately by the formula

$$\Delta S_C(\Gamma_e,x)=R(\Gamma_e)\Delta S_{id}(x) \ , \tag{33}$$

where

$$R(\Gamma_e)=0.7204-0.0354(\Gamma_e-10)+0.0016(\Gamma_e-10)^2$$

for $7\le\Gamma_e\le13$, and $\Delta S_{id}(x)$ has been given in Eq. (20). We depict Eqs. (20) and (33) also in Fig. 7, to show accuracy of the fitting formula (33).

IV. PHASE DIAGRAM FOR DENSE C-O MIXTURES

The evaluation of the thermodynamic quantities described in the preceding sections can be combined into a construction of the phase diagram for the C-O BIM's. Since the electrons form virtually incompressible background of neutralizing charges in the BIM material under investigation, the phase diagram is determined through the condition for minimization of Helmholtz free energy at constant T and n_e, the number density of electrons. The result of calculation, shown in Fig. 8, implies an

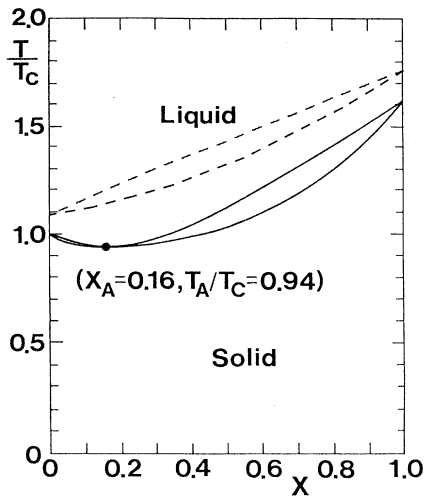

FIG. 8. Azeotropic phase diagram of C-O mixtures. The dashed curves are the spindle phase diagram of Ref. 24.

azeotropic phase diagram with the azeotropic point at $T_A = 0.94 T_C$ and $x_A = 0.16$.

The appearance of an azeotrope stems physically from the LM rule (6) and the mixing entropy (33) in solid. We remark that the increment of the internal energy between the mixed-alloy and chemically separated phases vanishes identically with the LM rule for both fluids and solids. Since $\Delta S_C < \Delta S_F$, the fluid phase is favored in the mixtures, resulting in lowering of the freezing temperatures. The solid state, still retaining a considerable amount of the mixing entropy (33), can sustain a mixed-alloy phase, rather than a chemically separated phase.

Stevenson's eutectic is a result of assuming the RAM rule (7) for solids [while assuming the LM rule (6) for liquids] and adopting the ideal entropy of mixing (20) for both fluids and solids. Near the freezing temperatures, the internal energy is overwhelmingly more the major constituent of the free energy than the entropy term. Since the RAM rule would substantially underestimate the magnitude of the BIM internal energy as Table 1 of Ref. 15 illustrates, the freezing temperatures would decrease and chemically separated phases would be favored over mixing alloys in solids. As we have shown in Sec. II, however, the assumption of the RAM rule (7) cannot be justified for the C-O BIM.

V. VARIATIONS OF MASS DENSITY ACROSS THE PHASE BOUNDARY

Variations of the mass density across the phase-boundary curves can be evaluated through a perturbative method.[9] In the ranges of physical parameters under present investigation, the partial pressure P_e of the electrons constitutes the bulk of the total pressure P of the system. The ionic contribution P_i then creates a difference in mass density between the coexisting solid-solution and fluid-mixture phases across the boundary.

In the first-order perturbation theory, the discontinuity,

$$\Delta\rho_m \equiv \rho_m(\text{solid}) - \rho_m(\text{fluid}) , \tag{34}$$

across the phase boundary is calculated as

$$\begin{aligned}\Delta\rho_m/\rho_m &= \Delta n_e/n_e - \Delta Y/Y \\ &= -\Delta P_i/\gamma P_e - \Delta Y/Y . \end{aligned} \tag{35}$$

Here $Y \equiv \langle Z \rangle / \langle A \rangle$ refers to the number of electrons per unit of atomic mass, and $\gamma \equiv (d \ln P_e / d \ln \rho_m)_Y$ is an adiabatic index.

The results for the azeotropic phase diagram of Fig. 8 are listed in Table 2 of Ref. 15. In the case of Stevenson's eutectic diagram, the discontinuities have been calculated[9] to fall in the range of $(1-2)\times 10^{-3}$ at the eutectic point. Hence, the present results at the azeotropic point are smaller by about an order of magnitude than those at Stevenson's eutectic point, predicting significantly reduced influences of the phase separation on the evolution of a C-O white dwarf.

VI. CONCLUDING REMARKS

We have theoretically investigated the thermodynamic functions for dense BIM materials through the MC simulations and by analytic means. We have in particular shown that the internal energies of the C-O BIM solids and fluids both obey accurately the LM formula (6), which, combined with an explicit evaluation (33) for the entropy of mixing in solids, has led to a prediction of an azeotropic phase diagram in Fig. 8.

A number of theoretical problems remain to be investigated, however, in conjunction with assumptions adopted in such a calculation of the phase diagram. Those include the following: accuracy and validity of the LM formula as applied to BIM's other than the C-O systems; utility of the simplified free-energy functionals[12] for the OCP when extended to the BIM; dependence on the modeling such as the Gaussian density waves and the long-range order parameter for the alloy; higher-order structural effects in the density-wave calculations; and possible deformation of crystalline structures due to $Z_1 \neq Z_2$. A treatment of any of those problems on a theoretically reliable basis would call for a work of considerable effort and will be a subject of future study.

After completion of this work and submittal of the manuscript, we became aware of a paper[24] by Barrat *et al.* on the same problem reporting calculations using a density-functional approach. They obtained an ordinary spindle-shaped phase diagram (dashed curves in Fig. 8), rather than an azeotropic one in the present work. As far as we can tell from Ref. 24, it appears that the present work is superior on three accounts. (1) Thermodynamic functions of the C-O mixtures have been examined carefully by performing MC simulations at relevant parametric combinations in white dwarfs for both solids and fluids. (2) We were able to characterize a possible long-

range order in the alloy phase by a third variational parameter ζ [see Eq. (27)]. (3) Freezing conditions have been formulated in an accurate way (see Ref. 12). It remains to be investigated which of the three has actually caused such a difference in the phase diagrams.

ACKNOWLEDGMENTS

This research was supported in part through Grants-in-Aid for Scientific Research provided by the Ministry of Education, Science, and Culture of Japan.

[1]S. Starrfield, J. W. Truran, W. M. Sparks, and G. S. Kutter, Astrophys. J. **176**, 169 (1972).

[2]J. Whelen and I. Iben, Astrophys. J. **186**, 1007 (1973).

[3]R. Canal and E. Schatzman, Astron. Astrophys. **46**, 229 (1976).

[4]D. A. Kirzhnitz, Zh. Eksp. Teor. Fiz. **38**, 503 (1960) [Sov. Phys. JETP—**11**, 365 (1960)].

[5]A. A. Abrikosov, Zh. Eksp. Teor. Fiz. **39**, 1798 (1960) [Sov. Phys. JETP—**12**, 1254 (1961)].

[6]E. E. Salpeter, Astrophys. J. **134**, 669 (1961).

[7]D. J. Stevenson, J. Phys. (Paris) Suppl. **41**, C2-61 (1980).

[8]R. Canal, J. Isern, and J. Labay, Nature **296**, 225 (1982).

[9]R. Mochkovitch, Astron. Astrophys. **122**, 212 (1983).

[10]J. L. Barrat, M. Baus, and J.-P. Hansen, J. Phys. C **20**, 1413 (1987).

[11]S. J. Smithline and A. D. J. Haymet, J. Chem. Phys. **86**, 6486 (1987).

[12]H. Iyetomi and S. Ichimaru, Phys. Rev. B **38**, 6761 (1988).

[13]H. Iyetomi and S. Ichimaru, Phys. Rev. A **25**, 2434 (1982); **27**, 3241 (1983).

[14]H. Iyetomi and S. Ichimaru, Phys. Rev. A **34**, 3203 (1986).

[15]A preliminary account of this research has been reported in S. Ichimaru, H. Iyetomi, and S. Ogata, Astrophys. J. Lett. **334**, L17 (1988).

[16]S. Ichimaru, H. Iyetomi, and S. Tanaka, Phys. Rep. **149**, 91 (1987).

[17]S. Ogata and S. Ichimaru, Phys. Rev. A **36**, 5451 (1987).

[18]S. G. Brush, H. L. Sahlin, and E. Teller, J. Chem. Phys. **45**, 2102 (1966).

[19]E. E. Salpeter, Aust. J. Phys. **7**, 373 (1954).

[20]S. Ichimaru, Rev. Mod. Phys. **54**, 1017 (1982).

[21]W. L. Slattery, G. D. Doolen, and H. E. DeWitt, Phys. Rev. A **26**, 2255 (1982).

[22]J.-P. Hansen, G. M. Torrie, and P. Vieillefosse, Phys. Rev. A **16**, 2153 (1977).

[23]T. Muto and Y. Takagi, in *Solid State Physics*, edited by F. Seitz and D. Turnbull (Academic, New York, 1955), Vol. 1, p. 193.

[24]J. L. Barrat, J.-P. Hansen, and R. Mochkovitch, Astron. Astrophys. **199**, L15 (1988).